iScience

CellPress
OPEN ACCESS

Article

A *BAP1* synonymous mutation results in exon skipping, loss of function and worse patient prognosis

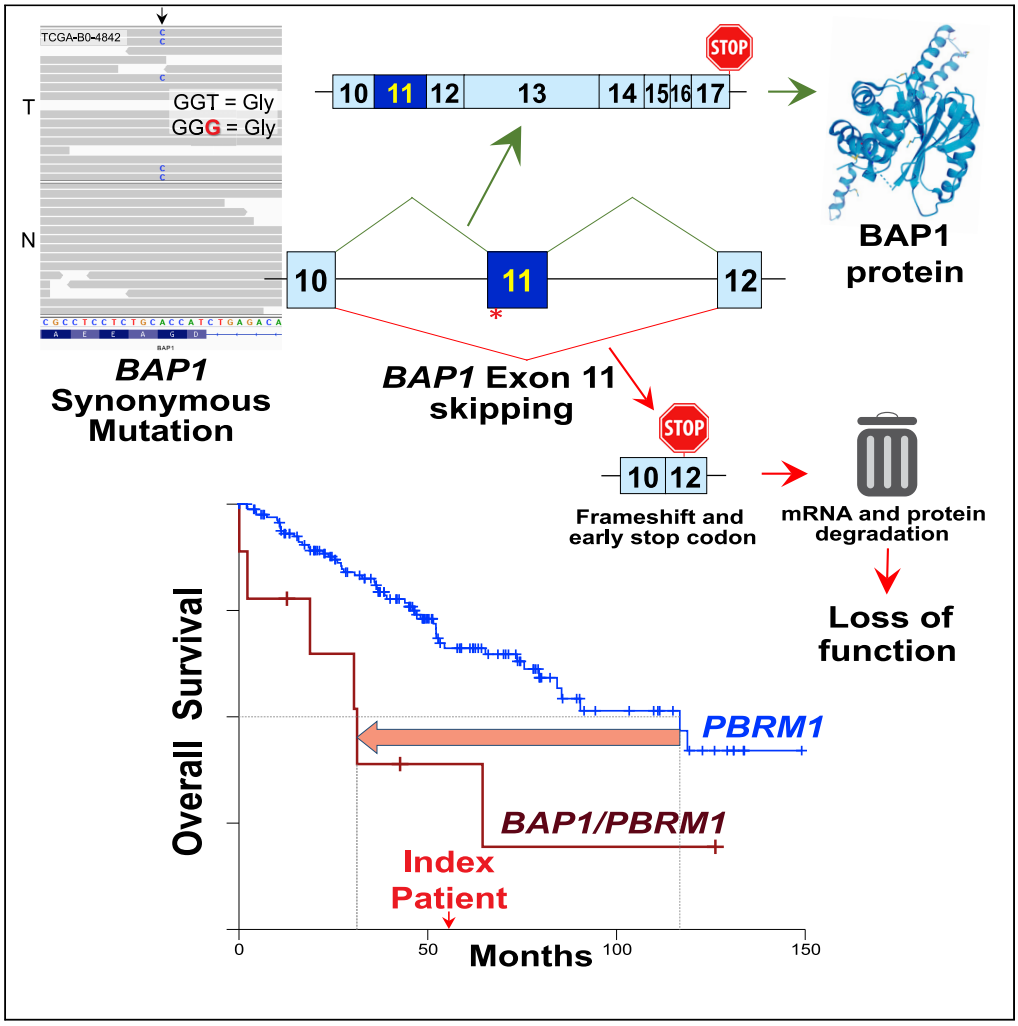

Jennifer Niersch, Silvia Vega-Rubín-de-Celis, Anna Bazarna, Svenja Mergener, Verena Jendrossek, Jens T. Siveke, Samuel Peña-Llopis

Samuel.Pena-Llopis@dkfz.de

HIGHLIGHTS

First synonymous *BAP1* mutation that leads to exon skipping and loss of function

Exon 11 skipping is a hotspot for BAP1 inactivation

First synonymous mutation reported to reduce fourfold the expected patient survival

Synonymous mutations can inactivate cancer genes and affect patient prognosis

Niersch et al., iScience 24, 102173
March 19, 2021
https://doi.org/10.1016/j.isci.2021.102173

iScience

CellPress
OPEN ACCESS

Article

A *BAP1* synonymous mutation results in exon skipping, loss of function and worse patient prognosis

Jennifer Niersch,[1,2,3,5] Silvia Vega-Rubín-de-Celis,[4,5] Anna Bazarna,[1,2,3] Svenja Mergener,[1,2,3] Verena Jendrossek,[4] Jens T. Siveke,[2,3] and Samuel Peña-Llopis[1,2,3,5,6,7,*]

SUMMARY

Synonymous mutations are generally disregarded by genomic analyses because they are considered non-pathogenic. We identified and characterized a somatic synonymous mutation in the epigenetic modifier and tumor suppressor *BAP1*, resulting in exon skipping and complete protein inactivation. This radically altered the prognosis of a clear-cell renal cell carcinoma patient from The Cancer Genome Atlas (TCGA) with a *PBRM1* mutation (a predictor biomarker for positive responses to immune checkpoint inhibitors) from good (an estimated overall survival of 117 months) to a very bad prognosis (an estimated overall survival of 31 months), emphasizing the importance of scrutinizing synonymous mutations near acceptor splice sites of cancer genes for accurate precision medicine.

INTRODUCTION

Cancer can be broadly defined as a collection of remarkably complex diseases caused by the accumulation of genomic and epigenetic modifications, such as mutations and chromatin alterations, which can be fatal when metastatic. For each tumor type, and preferably for each patient, it is essential to identify the 'driver' mutations that lead to tumor development among the 'passenger' mutations. Synonymous mutations alter the DNA sequence without changing the encoded amino acid of the resulting protein and, thus, are assumed as 'silent' and overlooked in many genomic studies.

Recent studies point out that synonymous mutations might affect the translation kinetics, mRNA stability, miRNA binding sites, or splicing machinery and ultimately alter protein function (Jayasinghe et al., 2018; Kimchi-Sarfaty et al., 2007; Sharma et al., 2019; Supek et al., 2014). In addition, synonymous mutations represent about 6–8% of all driver mutations by single-nucleotide variants in oncogenes (Supek et al., 2014). Overall, synonymous mutations (1) were found to be enriched in known cancer genes, (2) show a negative correlation of their frequency with the mutational load, indicating a selective pressure resulting in highly recurrent synonymous mutations, (3) are non-randomly distributed along the coding sequence and within internal exons and (4) differentially affect codons for specific amino acids (Sharma et al., 2019).

Kidney cancer is diagnosed annually in over 400,000 individuals and causes more than 175,000 deaths worldwide, being clear-cell renal cell carcinoma (ccRCC) the most frequent subtype (~75%) (Ricketts et al., 2018). An early event in ccRCC development is the inactivation of the pVHL pathway, followed by inactivating mutations of chromatin remodelers, such as *SETD2* (Dalgliesh et al., 2010) and *PBRM1* (Varela et al., 2011). We previously established that the deubiquitinase and epigenetic modifier BRCA1-associated protein 1 (*BAP1*) is a major driver of tumor development in ccRCC (Peña-Llopis et al., 2012) and its mutations are mutually exclusive with *PBRM1* (Peña-Llopis et al., 2012, 2013). Thus, tumors with *BAP1* mutations exhibit dismal prognosis and are characterized by aggressive features, including high tumor grade, mTORC1 activation (Peña-Llopis et al., 2012), rhabdoid and sarcomatoid histologies, tumor necrosis, and poor patient survival (Kapur et al., 2013). In contrast, patients with *PBRM1* mutations only (without *BAP1* mutations) have good prognosis and are characterized by low tumor grade, low mTORC1 activity (Peña-Llopis et al., 2012), and good overall survival (Kapur et al., 2013). Tumors with loss of BAP1 and PBRM1 showed the highest aggressiveness and shorter patient survival (Kapur et al., 2013; Peña-Llopis et al., 2012). Notably, several other research teams independently confirmed these discoveries (Creighton et al., 2013; Hakimi et al., 2013; Ricketts et al., 2018; Sato et al., 2013; Turajlic et al., 2018) and enabled the molecular genetic classification of this tumor

[1]Translational Genomics in Solid Tumors, German Cancer Consortium (DKTK) and German Cancer Research Center (DKFZ) at the University Hospital Essen, Hufelandstrasse 55, 45147 Essen, Germany

[2]Division of Solid Tumor Translational Oncology, German Cancer Consortium (DKTK) and German Cancer Research Center (DKFZ), Heidelberg, Germany

[3]Bridge Institute of Experimental Tumor Therapy, West German Cancer Center, University Hospital Essen, Essen, Germany

[4]Institute of Cell Biology (Cancer Research), University Hospital Essen, Essen, Germany

[5]These authors contributed equally

[6]Twitter: @Sam_PenaLlopis, @PenaLlopisLab

[7]Lead contact

*Correspondence: Samuel.Pena-Llopis@dkfz.de

https://doi.org/10.1016/j.isci.2021.102173

type based on inactivating mutations in *BAP1* and *PBRM1* (Kapur et al., 2013; Peña-Llopis et al., 2012), providing the rationale for precision medicine using subtype-specific therapies.

RESULTS

A somatic synonymous *BAP1* mutation leads to its loss of function and worsens patient prognosis

We identified a patient from The Cancer Genome Atlas (TCGA) kidney renal clear cell carcinoma (KIRC) (Creighton et al., 2013) whose tumor harbored 3p chromosomal loss (Figure S1) and a somatic nonsense *PBRM1* mutation. This patient (TCGA-B0-4842), a 73-year-old Caucasian woman, died 56 months after diagnosis. This was considerably rapid for a ccRCC patient with a *PBRM1* mutation, since an analysis of TCGA data showed a median overall survival of 117 months (95% confidence interval [CI]: 84–150 months) (Figure 1A). This relatively short survival was more similar to those patients with a *BAP1* mutation (median overall survival of 73 months [95% CI: 20–127 months]) or patients with mutations in both *BAP1* and *PBRM1* (median overall survival of 31 months [95% CI: 15–48 months]) (Figure 1A). Indeed, this patient revealed a somatic synonymous *BAP1* mutation near the acceptor splice site of exon 11 (c.936T>G, p.G312G) (Figure 1B).

Surprisingly, the tumor displayed low *BAP1* gene expression (Figure 1C) and one of the lowest BAP1 protein expressions among KIRC-TCGA patients (Figure S2B). A one-sample *t* test showed that the BAP1 protein expression of the index patient was closer to those of patients with mutations in *BAP1* or both *BAP1* and *PBRM1* ($p = 10^{-10}$ and 0.004, respectively) than patients with mutations in *PBRM1* ($p = 2 \cdot 10^{-103}$) or wild-type for these genes ($p = 3 \cdot 10^{-112}$) (Figure 1D). In addition, mTORC1 was highly active, as assessed by very high ribosomal protein S6 phosphorylation levels (Figures 1E and 1F). These levels, together with the highest tumor grade (grade 4) and pathologic stage III, are typically seen in patients with inactivating mutations in both *BAP1* and *PBRM1*, or only in *BAP1*, rather than just in *PBRM1* (Kapur et al., 2013; Peña-Llopis et al., 2012). Indeed, these levels were closer to tumors with *BAP1* or *BAP1/PBRM1* mutations than *PBRM1* mutations (Figure S2). Thereby, these data strongly suggest that the p.G312G synonymous *BAP1* mutation results in loss of BAP1 function and, consequently, higher tumor aggressiveness.

The synonymous *BAP1* mutation do not affect protein stability at the cDNA level

To understand the mechanism of inactivation of BAP1 expression caused by the synonymous mutation, we cloned the full-length cDNA of wild-type *BAP1* (or a catalytically inactivating p.C91S *BAP1* mutation) into pBABE-hygro vector to ensure a constitutive basal expression and we generated the c.936T>G, p.G312G mutation by site-directed mutagenesis (Figure 2A). We then reconstituted the BAP1-null ccRCC cell line UMRC-6 (or UM-RC-6) with wild-type *BAP1*, the p.G312G *BAP1* mutant or the p.C91S *BAP1* mutant constructs (and corresponding empty vector control). We observed similar total BAP1 protein levels (Figure 2B) and BAP1 protein stability upon blocking the protein synthesis with cycloheximide treatment in both wild-type *BAP1* and the p.G312G mutant (Figure 2C). We found similar results in a cholangiocarcinoma cell line, TFK-1, which had a nonsense mutation in *BAP1* (Figures 2C and 2E).

BAP1 targets the deubiquitination of histone H2A (Peña-Llopis et al., 2012; Scheuermann et al., 2010), and we observed that the synonymous p.G312G *BAP1* mutation deubiquitinated histone H2A to the same extent as the wild-type BAP1 (Figure 2F). However, UMRC-6 cells lacking *BAP1* or reconstituted with the p.C91S *BAP1* mutant showed strong ubiquitination of histone H2A, suggesting that the synonymous c.936T>G mutation in the full-length cDNA is not affecting the BAP1 deubiquitinating function.

We previously showed that the correlation of BAP1 loss with mTORC1 activation was not direct (Peña-Llopis et al., 2012). We analyzed several mTORC1 readouts, such as phosphorylated ribosomal protein S6 kinase (S6K), phosphorylated S6, and phosphorylated eukaryotic translation initiation factor 4E binding protein 1 (EIF4EBP1, also known as 4E-BP1), observed by changes in mobility shift by western blotting (Figure 2G). As expected, cells reconstituted with the p.G312G *BAP1* mutant showed similar mTORC1 activation as the wild-type and the p.C91S *BAP1* mutant in UMRC-6 (Figure 2G) and TFK-1 (Figure S3A) cells. Furthermore, cell proliferation of the p.G312G *BAP1* mutant cells was comparable to the wild-type *BAP1* and the p.C91S mutant, as well the empty vector control in UMRC-6 and TFK-1 cells (Figure S3B).

Taking together, these data suggest that the c.936T>G, p.G312G synonymous mutation is not affecting BAP1 at the cDNA level and the change of codon is not responsible for its inactivation.

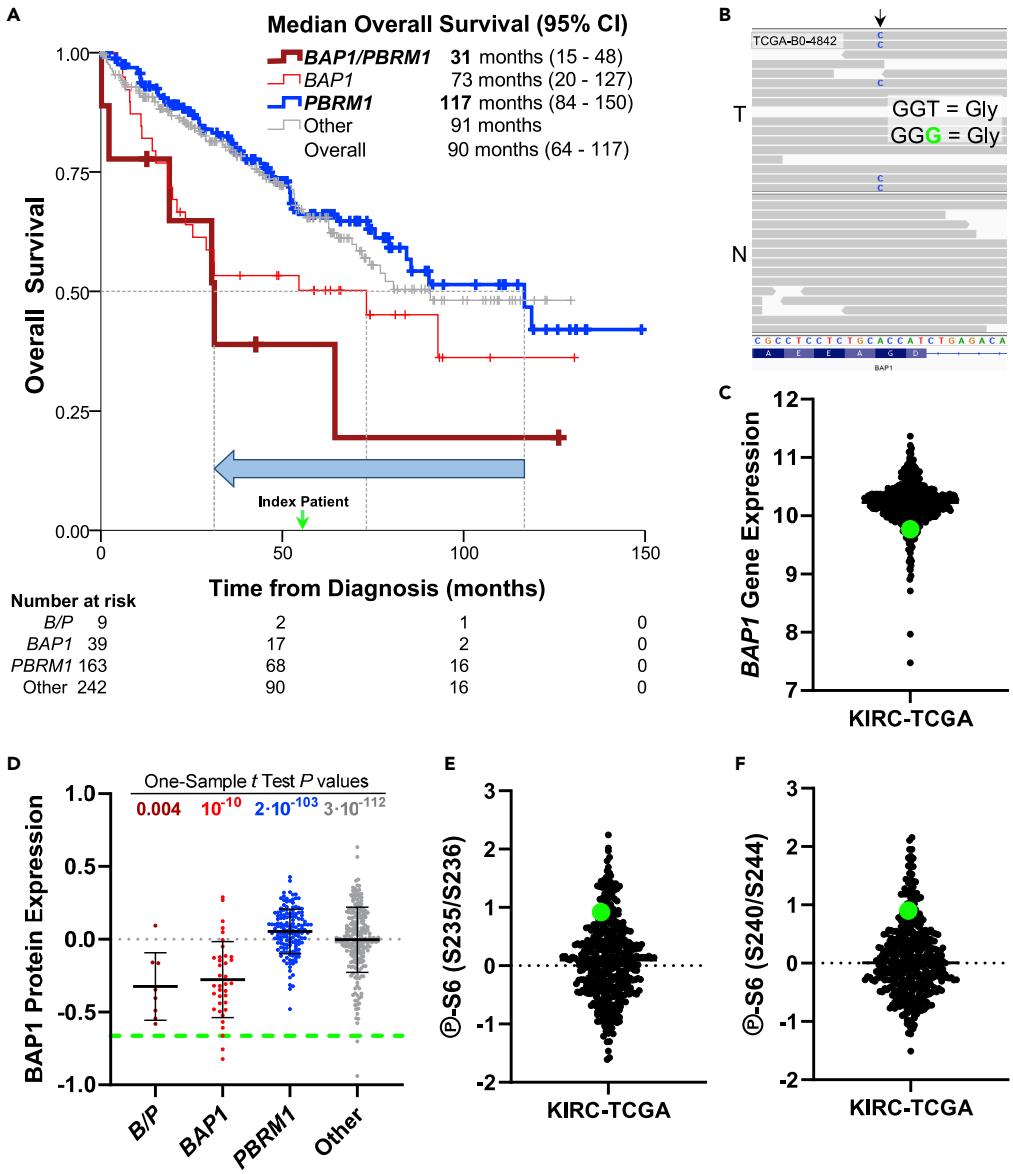

Figure 1. A somatic synonymous *BAP1* mutation leads to its loss of function and worsens patient prognosis

(A) Kaplan-Meier curves for the indicated groups from the KIRC-TCGA data set. The green arrow indicates the index patient. The blue arrow depicts the worsening of the median overall survival from tumors with *PBRM1* mutations to tumors with mutations in both *BAP1* and *PBRM1* (*B/P*).

(B) Genomic DNA sequence of the KIRC-TCGA patient displaying the somatic synonymous c.936T>G, p.G312G mutation in exon 11 of *BAP1* in the tumor (T) but not in the normal (N) kidney.

(C) Log2-transformed RNA-Seq Expectation-Maximization (RSEM) normalized gene expression for *BAP1* from KIRC-TCGA.

(D) Reverse phase protein array (RPPA) analysis for BAP1 from KIRC-TCGA stratifying for patients with *BAP1* and *PBRM1* mutations individually or for both genes (*B/P*). Index patient was compared with each group by the one-sample *t* test.

(E and F) Ribosomal protein S6 phosphorylation at S235/S236 (E) and at S240/S244 (F). For all plots, the green dot or dashed line indicates the index patient.

The synonymous *BAP1* mutation leads to exon skipping

Since the c.936T>G mutation is located 4 base pairs away from the acceptor splice site (Figure 1B), we next considered whether the synonymous mutation might affect the alternative splicing machinery, presumably by generating a new binding site for an exonic splicing silencer (Giulietti, 2013). Thus, we cloned exon 11 of

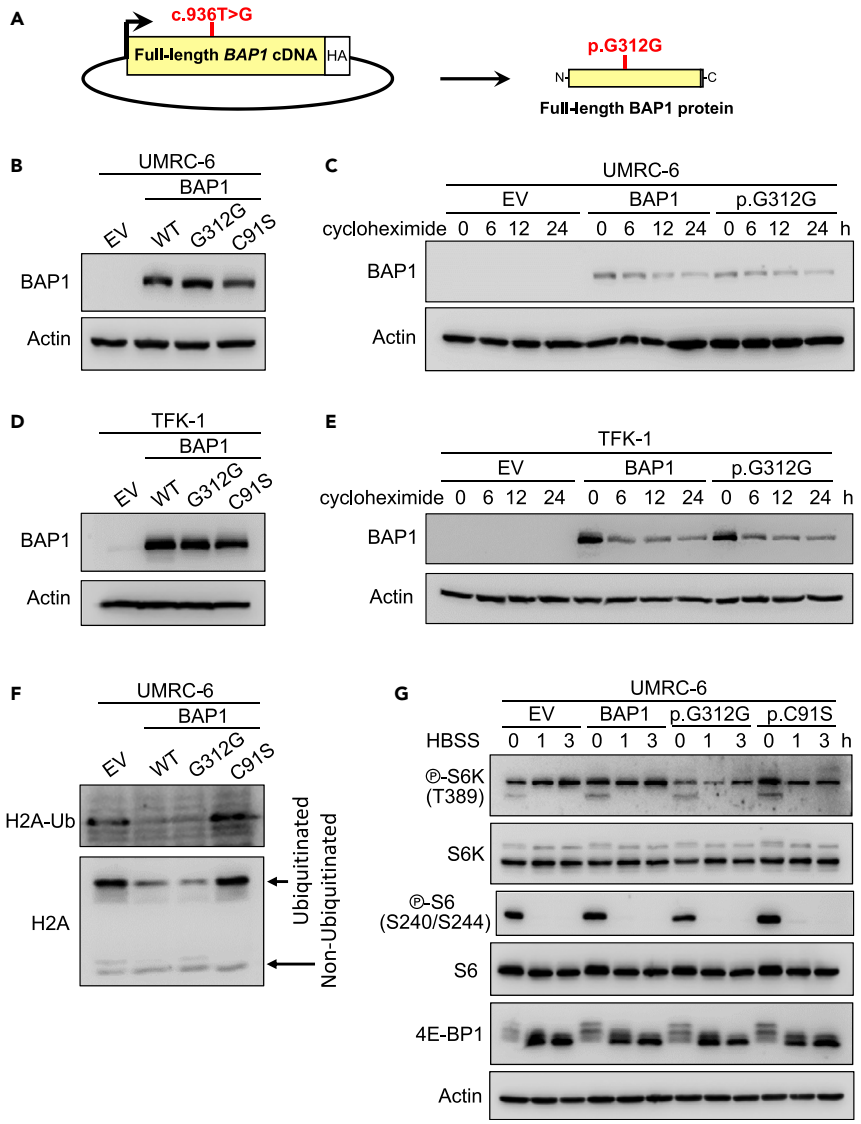

Figure 2. The synonymous *BAP1* mutation do not affect protein stability at the cDNA level

(A) Schema depicting the c.936T>G mutation in the full-length *BAP1* cDNA.

(B) UMRC-6 cells stably expressing the p.G312G *BAP1* mutant show by western blot similar total protein levels as cells reconstituted with wild-type (WT) *BAP1* or the p.C91S mutant. EV, empty vector.

(C) The decay over time of the protein encoded by the cDNA of the synonymous *BAP1* mutation is similar to the protein decay from the wild-type *BAP1* cDNA in UMRC-6 cells treated with 80 μg/ml of cycloheximide.

(D) BAP1-deficient cholangiocarcinoma TFK-1 cells reconstituted with the p.G312G *BAP1* mutant show similar levels of protein expression as wild-type or the p.C91S mutant *BAP1*.

(E) Western blot of the same stable TFK-1 cell lines treated with 10 μg/ml of cycloheximide for the indicated time shows similar protein decay for the p.G312G mutation as the wild-type *BAP1*.

(F) Reconstitution of UMRC-6 cells with the p.G312G mutation in *BAP1* decreases the ubiquitination of histone H2A to a similar level as to wild-type *BAP1*, but different than the p.C91S mutant or empty vector.

(G) UMRC-6 cells reconstituted with the p.G312G mutation show similar mTORC1 activation readouts in response to starvation as wild-type and the p.C91S mutant *BAP1*.

BAP1 into a bichromatic splicing minigene reporter (Orengo et al., 2006) to examine exon inclusion and exon skipping events in an *in vivo* splicing assay (Figure 3A). As a control, we cloned a *BAP1* synonymous mutation found in lung adenocarcinoma 6 base pairs away from the donor splice site in exon 7 (c.576C>T, p.D192D) obtained from the SynMICdb database (Sharma et al., 2019). These plasmids were transiently expressed in HeLa cells. Controls showed similar levels of exon integration and skipping, as assessed by

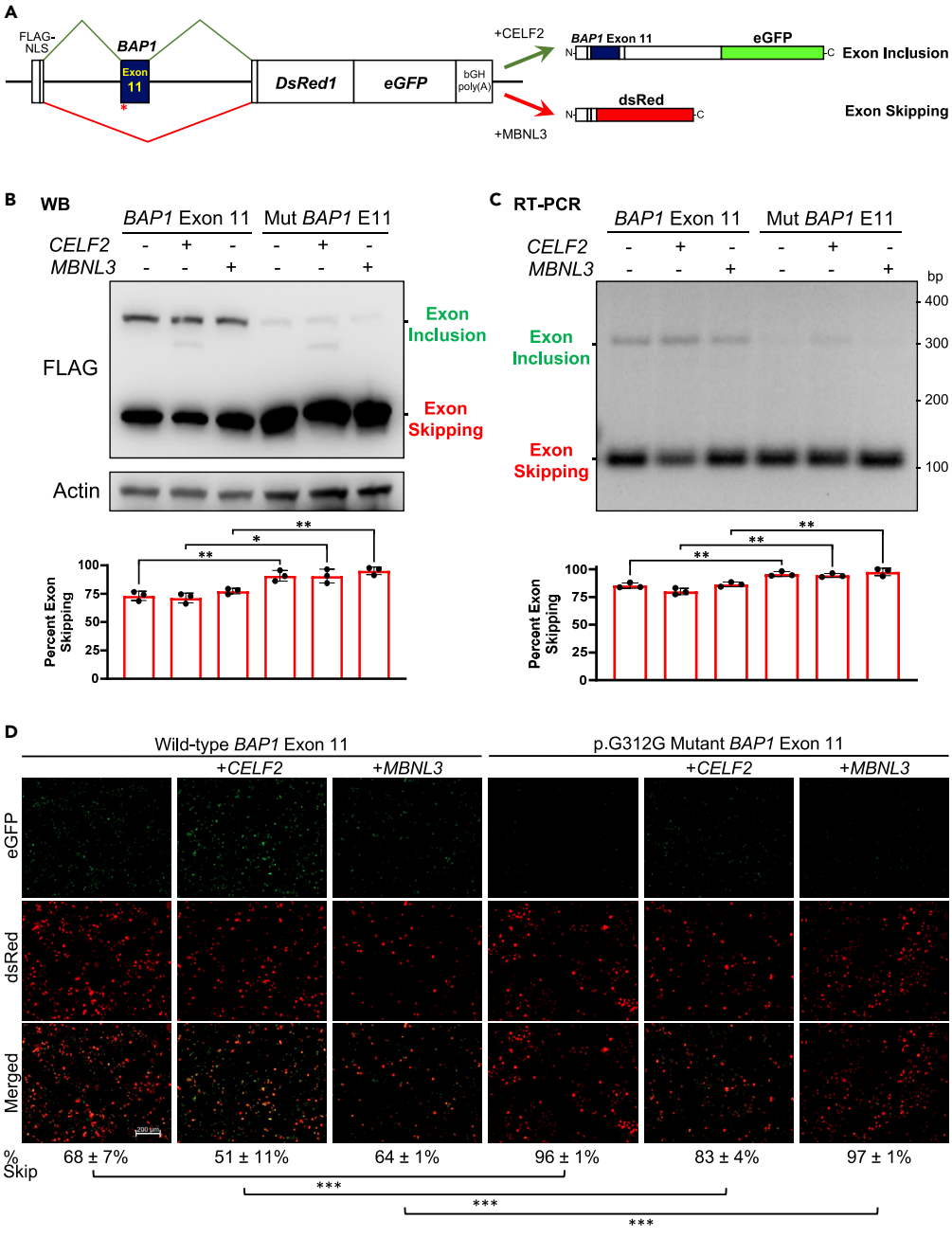

Figure 3. The synonymous *BAP1* mutation leads to exon skipping

(A) Diagram of the bichromatic alternative splicing reporter system to assess exon inclusion or skipping.

(B–D), *BAP1* exon 11 is skipped in HeLa cells transiently transfected with a minigene reporter containing the c.936T>G, p.G312G synonymous mutation whereas it is more inclusive with the wild-type exon 11, as indicated by western blotting of Flag-tagged proteins (B), RT-PCR (C) and fluorescence microscopy (D). Quantifications are the average ± SD of three independent experiments. *, p<0.05; **, p<0.01; ***, p<0.001. Scale bar represents 200 μm.

western blotting (Figure S5A), RT-PCR (Figure S5B) and fluorescence microscopy (Figure S5C). The co-expression of *CELF2* (also known as *ETR-3*) induced exon integration, whereas the co-expression of *MBNL3* induced exon skipping, as expected (Orengo et al., 2006).

Replacement of the synthetic exon by *BAP1* exon 7 resulted in exon integration, which was not affected by the c.576C>T mutation and only partially altered by the co-expression of *CELF2* and *MBNL3* (Figure S4).

However, the synonymous p.G312G mutation near the acceptor splice site at exon 11 showed striking exon skipping, quantified as 92% by western blotting (Figure 3B), 96% by RT-PCR (Figure 3C), and 92% by fluorescence microscopy (Figure 3D). Exon skipping of the p.G312G mutant *BAP1* was significantly higher than the wild-type *BAP1* exon 11 (74% [$p = 2 \cdot 10^{-7}$], 84% [$p = 5 \cdot 10^{-7}$], and 60% [$p = 2 \cdot 10^{-11}$], respectively). The degree of exon skipping difference between the wild-type and mutant sequence was then between 12 and 32%, which is similar to the 10-23% reduction of exon-skipping frequency previously reported for several oncogenes and *TP53* (Supek et al., 2014). Therefore, these data demonstrate that the synonymous c.936T>G, p.G312G *BAP1* mutation leads to exon 11 skipping. The fact that exon 11 was virtually completely excluded in the mutant and partially included in the wild-type *BAP1* suggests that exon 11 might be a potential bottleneck for BAP1 synthesis.

Clinical significance of *BAP1* exon 11 skipping

To get further insight into the clinical significance of *BAP1* exon 11 skipping, we analyzed the raw RNA-Seq data from the index patient. Unfortunately, the coverage was very poor and only two wild-type reads were observed between exon 10 and exon 11 and three reads between exon 11 and exon 12 of *BAP1* from two RNA-Seq tumor samples (Figure S6A). However, these reads did not contain the c.936T>G, p.G312G synonymous mutation, indicating that there is an extensive mRNA degradation of *BAP1*, in consonance with its low gene expression (Figure 1C). Thus, the wild-type reads proceed from the mixture of the RNA from the tumor with normal cells, such as stroma and infiltrating lymphocytes, as reflected at DNA level in Figures 1B and S1, and as we previously described in solid tumors but not in patient-derived xenografts, where human stroma is replaced by mouse stroma, which do not interfere and dilute the tumor DNA and RNA (Peña-Llopis et al., 2012). In addition, *BAP1* exon 11 skipping is predicted to result in protein frameshift and a premature stop codon (Figure S7), which can enhance mRNA decapping and the nonsense-mediated mRNA decay to selectively degrade imperfect mRNAs with early translation termination codons (Couttet and Grange, 2004; Muhlrad and Parker, 1994). Consistent with this notion, similar wild-type reads were observed in *PBRM1*, which harbored a nonsense mutation, but not in adjacent genes (Figure S6B). Therefore, the lack of *BAP1* mutant mRNA reads in the index patient (Figure S6A) agrees with the nonsense-mediated mRNA decay caused by premature translation termination codon due to exon 11 skipping.

Unexpectedly, a close examination of the eight KIRC-TCGA patients with splice-site mutations in *BAP1* revealed that two patients had mutations in the acceptor splice site of *BAP1* exon 11. TCGA-BP-4798 showed a c.IVS932-2A>G mutation that was considered likely pathogenic according to dbSNP database (rs112194987) and resulted in exon 11 skipping, as evidenced by RNA-Seq reads between exons 10 and 12 (Figure 4A). TCGA-CZ-5985 showed a c.IVS932-1G>T mutation (rs9848343 in dbSNP) and solid evidence for exon 11 skipping with 4 reads between exons 10 and 12 (Figure 4B). Similar to the index patient, both splice-site mutations resulted in low *BAP1* gene expression (Figure 4C) and BAP1 protein expression (Figure 4D), especially for TCGA-CZ-5985, which displayed the second lowest BAP1 levels from KIRC-TCGA. In addition, ribosomal protein S6 expression (Figure 4E) and phosphorylation levels (Figure 4F) were high, as expected to be found in patients with BAP1 loss.

Considering that there are 32 splicing sites among the 17 exons of *BAP1*, the fact of finding 2 of 8 patients with splice-site mutations in the acceptor splice site of exon 11 is very unlikely by chance alone ($p = 0.0015$), according to a cumulative binomial distribution. This suggests that exon 11 skipping might be a hotspot for BAP1 inactivation.

The clinical significance of exon 11 skipping is, however, more complicated. Patient TCGA-BP-4798 harbored an additional missense mutation in *TP53* and showed distant metastasis at diagnosis, dying almost 11 months thereafter, whereas patient TCGA-CZ-5985 was still alive 65 months after diagnosis. This suggests that despite having a similar *BAP1* mutation and inactivation, other alterations contribute decisively in the patient prognosis, such as an additional *PBRM1* mutation in the index patient and a *TP53* mutation in TCGA-BP-4798.

In summary, we have strong evidence to claim that the somatic synonymous mutation in *BAP1* of the index patient results in exon 11 skipping, frameshift and premature stop codon, leading to mRNA and protein degradation and ultimately, together with chromosome 3p loss, to the complete loss of function for BAP1 (Figure 4G). The inactivation of BAP1 contributed to a shorter survival than the one that would be expected for a patient with ccRCC with a *PBRM1* mutation.

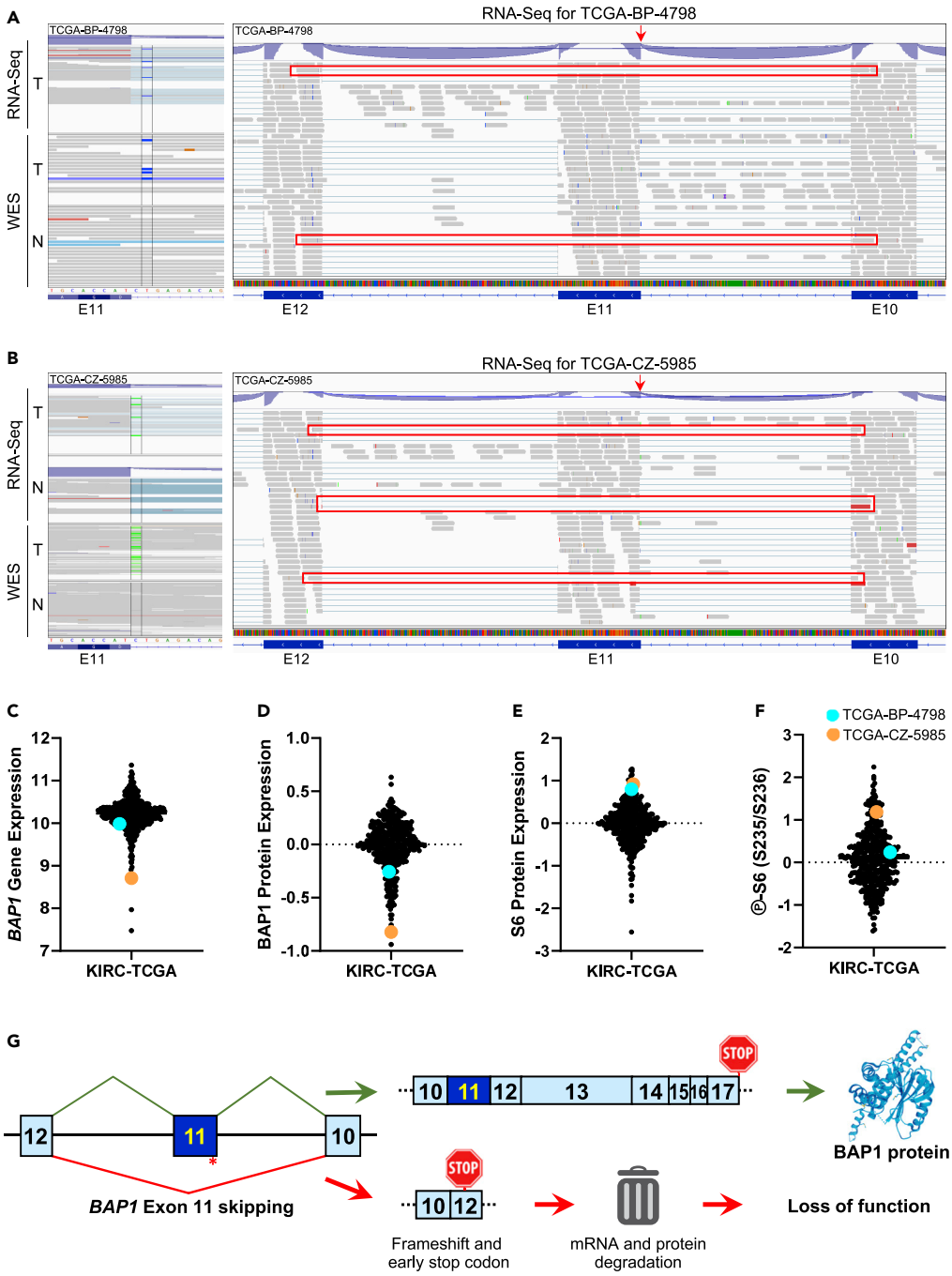

Figure 4. Mutations in the acceptor splice site of *BAP1* exon 11 lead to exon skipping and loss of function

(A) Patient TCGA-BP-4798 has a somatic mutation in the acceptor splice site of exon 11 (c.IVS932-2A>G) as depicted by whole-genome sequencing (WES) and RNA-Seq of the tumor (T) but not normal kidney (N) WES. Exon 11 skipping for patient TCGA-BP-4798 is evidenced by RNA-Seq reads spanning from exon 10 to exon 12 and highlighted in red. The red arrow indicates the splice-site mutation.

(B) Patient TCGA-CZ-5985 has a somatic mutation in the acceptor splice site of exon 11 (c.IVS932-1G>T) as depicted by whole-genome sequencing (WES) and RNA-Seq of the tumor (T) but not normal kidney (N). Exon 11 skipping for patient TCGA-CZ-5985 is indicated by RNA-Seq reads spanning from exon 10 to exon 12 and highlighted in red. The red arrow indicates the splice-site mutation.

Figure 4. *Continued*
(C–F) Log2-transformed RNA-Seq RSEM normalized gene expression for *BAP1* (C), RPPA for BAP1 (D), total ribosomal protein S6 expression (E) and S6 phosphorylation at S235/S236 (F) from KIRC-TCGA for patients TCGA-BP-4798 (in cyan) and TCGA-CZ-5985 (in orange).
(G) Diagram illustrating the summary of this study, where a synonymous mutation near the acceptor splice site of exon 11 of BAP1 leads to exon skipping, frameshift and premature stop codon, inducing its mRNA and protein degradation and loss of function.

DISCUSSION

We describe here a patient with renal cell carcinoma with presumably good prognosis due to a *PBRM1* mutation, who experienced a relatively short survival by harboring an additional unacknowledged inactivating synonymous mutation in *BAP1*.

The tumor with the synonymous p.G312G mutation in *BAP1* showed low gene expression and one of the lowest protein expressions from KIRC-TCGA, suggesting loss of function, as evidenced by phosphorylation of ribosomal protein S6, which is associated with BAP1 loss (Kapur et al., 2013; Peña-Llopis et al., 2012). However, reconstitution of BAP1-deficient ccRCC and cholangiocarcinoma cell lines with the c.936T>G *BAP1* mutation in the full-length cDNA showed similar protein levels, stability and histone H2A deubiquitination as the wild-type *BAP1*, proving that the synonymous mutation is not disrupting *BAP1* at the cDNA level. Interestingly, the synonymous mutation was near the acceptor splice site of exon 11. Thus, we cloned this exon into a sophisticated bichromatic *in vivo* splicing system (Orengo et al., 2006) and demonstrated by western blotting, RT-PCR, and fluorescent microscopy that the *BAP1* synonymous mutation resulted in exon 11 skipping. Remarkably, two of eight patients with splice-site *BAP1* mutations from KIRC-TCGA showed mutations in the acceptor splice site of exon 11, suggesting that exon 11 skipping might be a hotspot for BAP1 inactivation. It is well known that frameshift mutations leading to premature termination of translation can cause rapid mRNA degradation to prevent the production of non-functional or toxic truncated proteins (Couttet and Grange, 2004; Muhlrad and Parker, 1994). Hence, we provide here strong evidence to support that the c.936T>G, p.G312G synonymous mutation in *BAP1* results in exon 11 skipping, frameshift, premature stop codon, mRNA degradation, protein loss and, eventually, loss of function, which contributed negatively to decrease almost fourfold the expected patient survival (from 117 to 31 months).

This study has clinical relevance, since *PBRM1* mutations were reported to be predictive biomarkers for positive responses to immune checkpoint inhibitors in renal cell carcinoma (Braun et al., 2019; Miao et al., 2018). However, recent clinical trials in advanced renal cell carcinoma showed no association of *PBRM1* mutations with progression-free survival (Motzer et al., 2020). Furthermore, a recent study failed to associate the inactivation of several genes of the mammalian Switch/Sucrose Non-Fermentable (mSWI/SNF) with clinical outcomes in patients with cancer treated with systemic immune checkpoint inhibitors, except *PBRM1* in ccRCC (Abou Alaiwi et al., 2020). Therefore, the clinical benefits observed by treatment with immune checkpoint inhibitors in patients with ccRCC with *PRBM1* mutations, most likely are simply because, as we previously described, they are mutually exclusive of *BAP1* mutations (Peña-Llopis et al., 2012, 2013), which displayed poor overall patient survival (Kapur et al., 2013). Thus, *PBRM1* mutation should not be taken solely as a predictive marker in ccRCC but rather in combination with potential BAP1 inactivation (by DNA sequencing and/or immunohistochemistry) (Peña-Llopis et al., 2012) to have a more complete picture for each patient, fostering an accurate identification of the individual cancer driver genes and facilitating precision oncology.

A *BAP1* missense mutation (p.N78S), but not a synonymous mutation, was recently found to lead to alternative splicing (Jayasinghe et al., 2018). By comparing immunohistochemistry with mutation data, we previously showed that all frameshift mutations (11/11) and 85% (11/13) of point mutations in *BAP1* were unable to be translocated to the nucleus in ccRCC tumors, indicating loss of function (Peña-Llopis et al., 2012). The two missense mutations that showed nuclear BAP1 expression had mutations in the catalytic site of binding to ubiquitin and the binding to the ULD domain, respectively, and thus unlikely to be functional (Peña-Llopis et al., 2012). In addition, all tumors with *BAP1* mutations are accompanied by chromosomal 3p loss. Thus, the only allele left is the one with the mutation. Therefore, to our knowledge, this study provides the first evidence of a synonymous mutation in *BAP1* that leads to exon skipping and protein inactivation. This work also delivers insight into an unappreciated mechanism of inactivation of a very important tumor suppressor, which is frequently mutated and drives tumorigenesis in many cancer entities besides ccRCC (Peña-Llopis et al., 2012), including uveal melanoma (Harbor et al., 2010), mesothelioma (Bott et al., 2011),

and cholangiocarcinoma (Jiao et al., 2013). Remarkably, synonymous mutations toward the 5′ end of coding sequences were shown to be depleted but exhibited more pronounced predicted structural impact, suggesting higher selective pressure in this region (Sharma et al., 2019). The database of synonymous mutations in cancer (SynMICdb) recently generated (Sharma et al., 2019) could be a good resource for assessing the potential impact of specific synonymous mutations. Hence, synonymous mutations identified in clinical samples should not be systematically discarded but carefully analyzed in cancer genes, especially near the acceptor splice sites.

Limitations of the study

A limitation of this study is that we are analyzing the expression of an exogenous minigene. However, it was previously shown to be a reliable system for claiming that certain mutations affected splicing (Jayasinghe et al., 2018; Supek et al., 2014), observing similar ratios of exon inclusion/exclusion as we report here.

Resource availability

Lead contact

Further information and requests for resources and reagents should be directed to and will be fulfilled by the lead contact, Samuel Peña-Llopis (Samuel.Pena-Llopis@dkfz.de).

Materials availability

Plasmids generated in this study were deposited to Addgene (https://www.addgene.org/browse/article/28211439). Stable cell lines generated in this study will be deposited at the German Collection of Microorganisms and Cell Cultures (DSMZ) upon manuscript acceptance.

Data and code availability

This study did not generate any unique data sets or code.

METHODS

All methods can be found in the accompanying Transparent methods supplemental file.

SUPPLEMENTAL INFORMATION

Supplemental information can be found online at https://doi.org/10.1016/j.isci.2021.102173.

ACKNOWLEDGMENTS

We thank TCGA for sharing their data and Prof. Benedikt Brors, Dr. Martina Fröhlich, and Dr. Jules Kerssemakers for facilitating access to genomic raw data, as well as Prof. Stefan Fröhling and Dr. Stephanie Rössler for kindly providing cells. This project has received funding from the German Cancer Consortium (DKTK), the European Union's Horizon 2020 research and innovation program under the Marie Skłodowska-Curie Grant Agreement No. 798637 and a grant from the German Research Foundation (DFG) (PE 2696/1-1) to S.P.-L. S.V.-R. was supported by an NCT-DKTK School of Oncology Fellowship and a DFG grant (VE1153/1-1). J.T.S. was supported by a DFG grant (SI1549/3-1, Clinical Research Unit KFO337), through the Collaborative Research Center SFB824 (project C4), and the German Cancer Aid (70112505; PIPAC consortium).

AUTHOR CONTRIBUTIONS

J.N., A.B., and S.M. performed experiments. S.V.-R. designed and performed experiments and revised the manuscript. V.J. and J.T.S. provided resources, feedback, and revised the manuscript. S.P.-L. conceived the study, designed experiments, performed the bioinformatics and statistical analyses, supervised the project, and wrote the manuscript.

DECLARATION OF INTERESTS

J.T.S. reports personal fees from AstraZeneca, Baxalta, Immunocore, Novartis, Shire; research grants (institutional) and personal fees from Bristol-Myers Squibb, Celgene, Roche; ownership from FAPI holding (<3%); board membership from Pharma15, outside the submitted work.

Received: May 15, 2020
Revised: October 11, 2020
Accepted: February 8, 2021
Published: March 19, 2021

REFERENCES

Abou Alaiwi, S., Nassar, A.H., Xie, W., Bakouny, Z., Berchuck, J.E., Braun, D.A., Baca, S.C., Nuzzo, P.V., Flippot, R., Mouhieddine, T.H., et al. (2020). Mammalian SWI/SNF complex genomic alterations and immune checkpoint blockade in solid tumors. Cancer Immunol. Res. *8*, 1075–1084.

Bott, M., Brevet, M., Taylor, B.S., Shimizu, S., Ito, T., Wang, L., Creaney, J., Lake, R.A., Zakowski, M.F., Reva, B., et al. (2011). The nuclear deubiquitinase BAP1 is commonly inactivated by somatic mutations and 3p21.1 losses in malignant pleural mesothelioma. Nat. Genet. *43*, 668–672.

Braun, D.A., Ishii, Y., Walsh, A.M., Van Allen, E.M., Wu, C.J., Shukla, S.A., and Choueiri, T.K. (2019). Clinical validation of *PBRM1* alterations as a marker of immune checkpoint inhibitor response in renal cell carcinoma. JAMA Oncol. *5*, 1631–1633.

Couttet, P., and Grange, T. (2004). Premature termination codons enhance mRNA decapping in human cells. Nucleic Acids Res. *32*, 488–494.

Creighton, C.J., Morgan, M., Gunaratne, P.H., Wheeler, D.A., Gibbs, R.A., Gordon Robertson, A., Chu, A., Beroukhim, R., Cibulskis, K., Signoretti, S., et al. (2013). Comprehensive molecular characterization of clear cell renal cell carcinoma. Nature *499*, 43–49.

Dalgliesh, G.L., Furge, K., Greenman, C., Chen, L., Bignell, G., Butler, A., Davies, H., Edkins, S., Hardy, C., Latimer, C., et al. (2010). Systematic sequencing of renal carcinoma reveals inactivation of histone modifying genes. Nature *463*, 360–363.

Giulietti, M., et al. (2013). SpliceAid-F: a database of human splicing factors and their RNA-binding sites. Nucleic Acids Res. https://doi.org/10.1093/nar/gks997.

Hakimi, A.A., Ostrovnaya, I., Reva, B.A., Schultz, N., Chen, Y.B., Gonen, M., Liu, H., Takeda, S., Voss, M.H., Tickoo, S.K., et al. (2013). Adverse outcomes in clear cell renal cell carcinoma with mutations of 3p21 epigenetic regulators BAP1 and SETD2: a report by MSKCC and the KIRC TCGA research network. Clin. Cancer Res. *19*, 3259–3267.

Harbour, J.W., Onken, M.D., Roberson, E.D., Duan, S., Cao, L., Worley, L.A., Council, M.L., Matatall, K.A., Helms, C., and Bowcock, A.M. (2010). Frequent mutation of *BAP1* in metastasizing uveal melanomas. Science *330*, 1410–1413.

Jayasinghe, R.G., Cao, S., Gao, Q., Wendl, M.C., Vo, N.S., Reynolds, S.M., Zhao, Y., Climente-Gonzalez, H., Chai, S., Wang, F., et al. (2018). Systematic analysis of splice-site-creating mutations in cancer. Cell Rep. *23*, 270–281 e273.

Jiao, Y., Pawlik, T.M., Anders, R.A., Selaru, F.M., Streppel, M.M., Lucas, D.J., Niknafs, N., Guthrie, V.B., Maitra, A., Argani, P., et al. (2013). Exome sequencing identifies frequent inactivating mutations in *BAP1*, *ARID1A* and *PBRM1* in intrahepatic cholangiocarcinomas. Nat. Genet. *45*, 1470–1473.

Kapur, P., Peña-Llopis, S., Christie, A., Zhrebker, L., Pavia-Jimenez, A., Rathmell, W.K., Xie, X.J., and Brugarolas, J. (2013). Effects on survival of *BAP1* and *PBRM1* mutations in sporadic clear-cell renal-cell carcinoma: a retrospective analysis with independent validation. Lancet Oncol. *14*, 159–167.

Kimchi-Sarfaty, C., Oh, J.M., Kim, I.W., Sauna, Z.E., Calcagno, A.M., Ambudkar, S.V., and Gottesman, M.M. (2007). A "silent" polymorphism in the MDR1 gene changes substrate specificity. Science *315*, 525–528.

Miao, D., Margolis, C.A., Gao, W., Voss, M.H., Li, W., Martini, D.J., Norton, C., Bosse, D., Wankowicz, S.M., Cullen, D., et al. (2018). Genomic correlates of response to immune checkpoint therapies in clear cell renal cell carcinoma. Science *359*, 801–806.

Motzer, R.J., Robbins, P.B., Powles, T., Albiges, L., Haanen, J.B., Larkin, J., Mu, X.J., Ching, K.A., Uemura, M., Pal, S.K., et al. (2020). Avelumab plus axitinib versus sunitinib in advanced renal cell carcinoma: biomarker analysis of the phase 3 JAVELIN Renal 101 trial. Nat. Med. *26*, 1733–1741.

Muhlrad, D., and Parker, R. (1994). Premature translational termination triggers mRNA decapping. Nature *370*, 578–581.

Orengo, J.P., Bundman, D., and Cooper, T.A. (2006). A bichromatic fluorescent reporter for cell-based screens of alternative splicing. Nucleic Acids Res. *34*, e148.

Peña-Llopis, S., Christie, A., Xie, X.J., and Brugarolas, J. (2013). Cooperation and antagonism among cancer genes: the renal cancer paradigm. Cancer Res. *73*, 4173–4179.

Peña-Llopis, S., Vega-Rubín-de-Celis, S., Liao, A., Leng, N., Pavía-Jiménez, A., Wang, S., Yamasaki, T., Zhrebker, L., Sivanand, S., Spence, P., et al. (2012). BAP1 loss defines a new class of renal cell carcinoma. Nat. Genet. *44*, 751–759.

Ricketts, C.J., De Cubas, A.A., Fan, H., Smith, C.C., Lang, M., Reznik, E., Bowlby, R., Gibb, E.A., Akbani, R., Beroukhim, R., et al. (2018). The cancer genome Atlas comprehensive molecular characterization of renal cell carcinoma. Cell Rep. *23*, 313–326.

Sato, Y., Yoshizato, T., Shiraishi, Y., Maekawa, S., Okuno, Y., Kamura, T., Shimamura, T., Sato-Otsubo, A., Nagae, G., Suzuki, H., et al. (2013). Integrated molecular analysis of clear-cell renal cell carcinoma. Nat. Genet. *45*, 860–867.

Scheuermann, J.C., de Ayala Alonso, A.G., Oktaba, K., Ly-Hartig, N., McGinty, R.K., Fraterman, S., Wilm, M., Muir, T.W., and Muller, J. (2010). Histone H2A deubiquitinase activity of the Polycomb repressive complex PR-DUB. Nature *465*, 243–247.

Sharma, Y., Miladi, M., Dukare, S., Boulay, K., Caudron-Herger, M., Gross, M., Backofen, R., and Diederichs, S. (2019). A pan-cancer analysis of synonymous mutations. Nat. Commun. *10*, 2569.

Supek, F., Minana, B., Valcarcel, J., Gabaldon, T., and Lehner, B. (2014). Synonymous mutations frequently act as driver mutations in human cancers. Cell *156*, 1324–1335.

Turajlic, S., Xu, H., Litchfield, K., Rowan, A., Horswell, S., Chambers, T., O'Brien, T., Lopez, J.I., Watkins, T.B.K., Nicol, D., et al. (2018). Deterministic evolutionary trajectories influence primary tumor growth: TRACERx renal. Cell *173*, 595–610.

Varela, I., Tarpey, P., Raine, K., Huang, D., Ong, C.K., Stephens, P., Davies, H., Jones, D., Lin, M.L., Teague, J., et al. (2011). Exome sequencing identifies frequent mutation of the SWI/SNF complex gene *PBRM1* in renal carcinoma. Nature *469*, 539–542.

iScience, Volume *24*

Supplemental information

A *BAP1* synonymous mutation results in exon skipping, loss of function and worse patient prognosis

Jennifer Niersch, Silvia Vega-Rubín-de-Celis, Anna Bazarna, Svenja Mergener, Verena Jendrossek, Jens T. Siveke, and Samuel Peña-Llopis

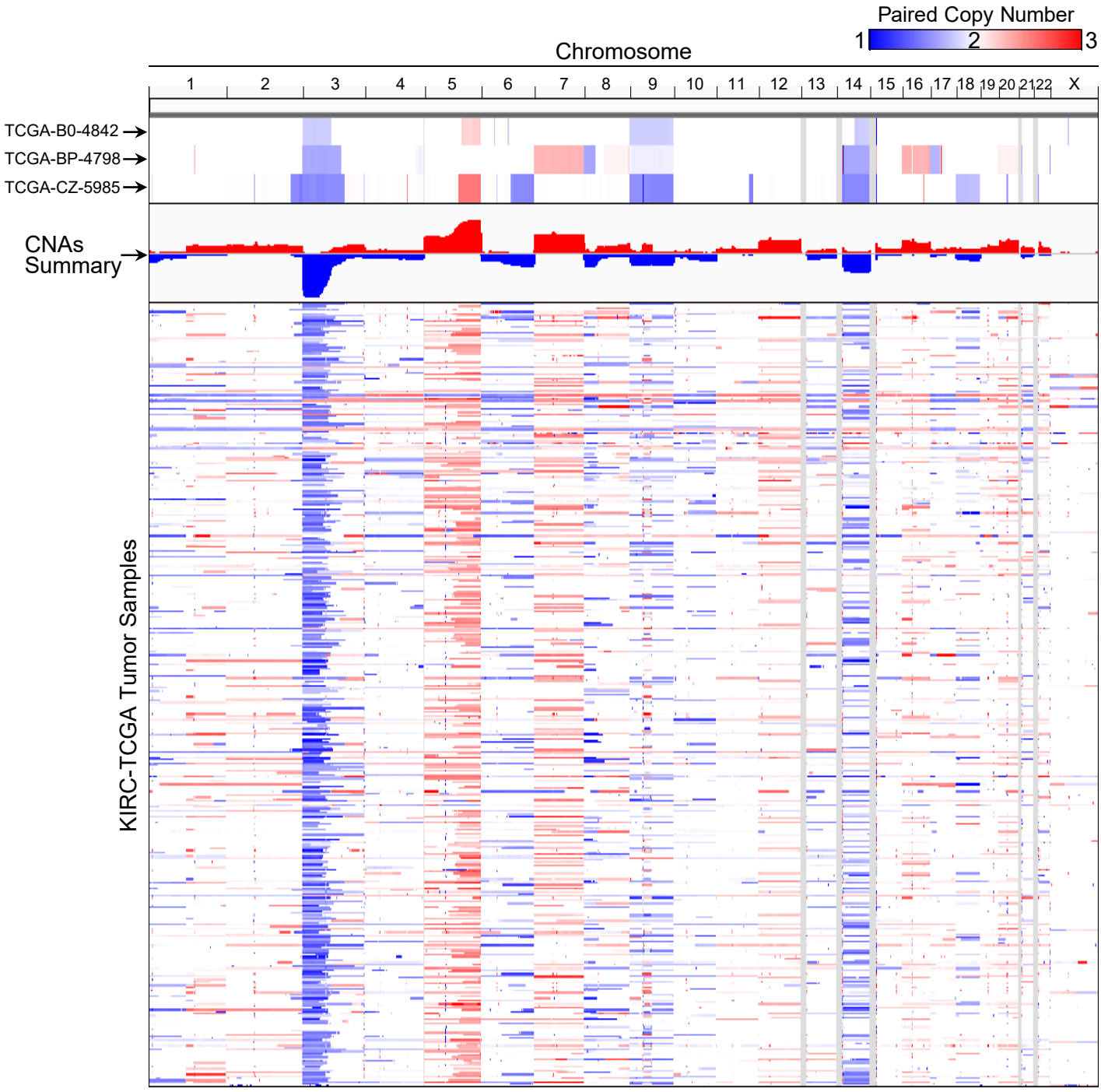

Figure S1. Index patient (TCGA-B0-4842) and patients with splice-site mutations in *BAP1* exon 11 (TCGA-BP-4798 and TCGA-CZ-5985) display representative copy number alterations (CNAs) of clear-cell renal cell carcinoma, Related to Figure 1. The copy numbers of the index patient are 1.7 for copy number loss and 2.3 for copy number gain instead of 1 and 3, respectively, indicating that about 30% of the DNA comes from the tumor and 70% comes from normal cells that contaminated the tumor. For TCGA-BP-4798 and TCGA-CZ-5985, ~40% and ~50% of DNA, respectively, come from the tumor. CNAs were obtained from KIRC-TCGA and visualized with Integrative Genomics Viewer (IGV).

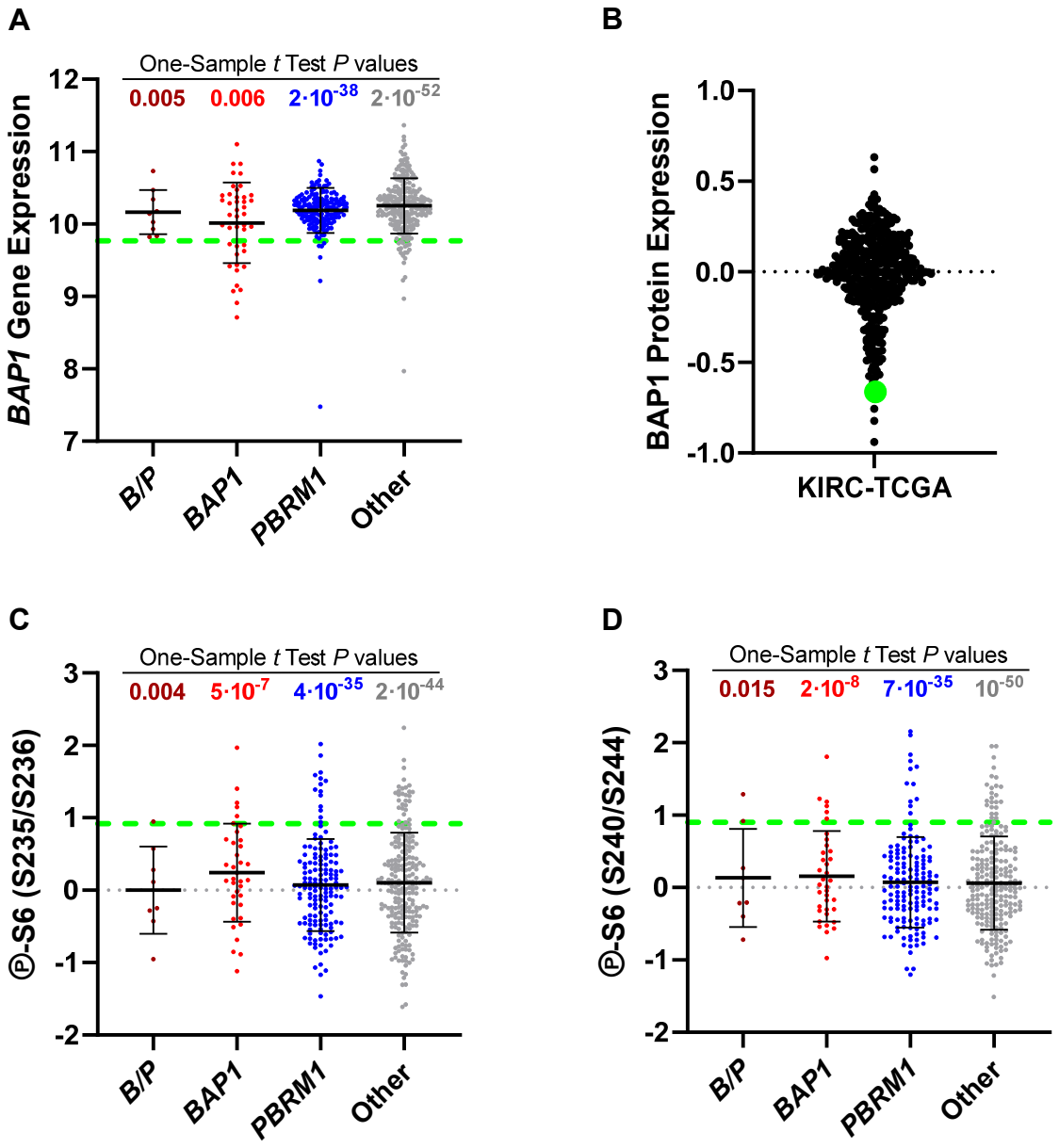

Figure S2. The tumor of the index patient with the synonymous p.G312G mutation in *BAP1* displays more similarities to tumors with *BAP1* or *BAP1/PBRM1* (*B/P*) mutations than those with *PBRM1* mutations, Related to Figure 1. **(A)** Log2-transformed RNA-Seq Expectation-Maximization (RSEM) normalized gene expression for *BAP1* from KIRC-TCGA stratifying for patients with *BAP1* and *PBRM1* mutations individually or for both genes (*B/P*). Index patient was compared with each group by the one-sample *t* test. (**B**) Reverse phase protein array (RPPA) for BAP1 from KIRC-TCGA. (**C-D**) Ribosomal protein S6 phosphorylation at S235/S236 (**C**) and at S240/S244 (**D**). For all plots, the green or dashed line dot indicates the index patient.

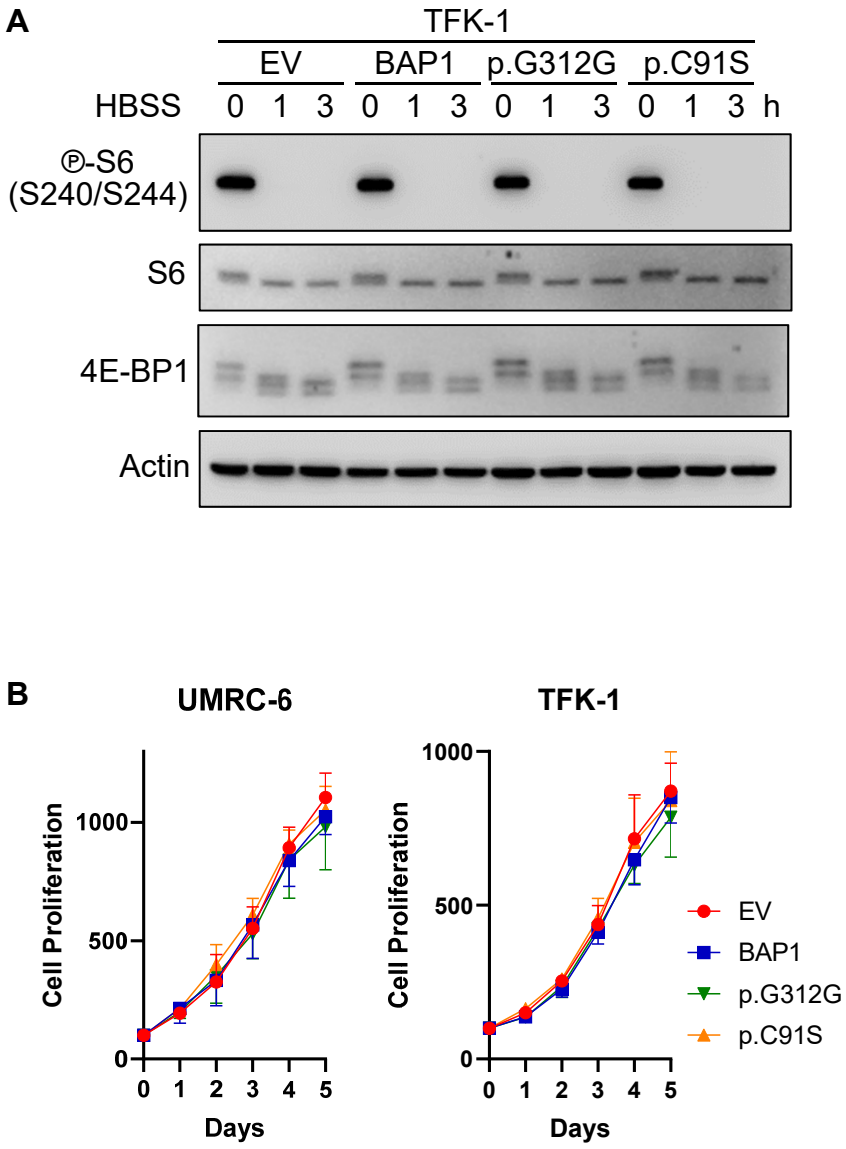

Figure S3. There are no significant differences between the p.G312G synonymous mutation and the wild-type, p.C91S mutant *BAP1* or empty vector in the response to starvation and cell proliferation, Related to Figure 2. (**A**) Western blotting for mTORC1 activation readouts in TFK-1 cells starved with HBSS for the indicated time. (**B**) Cell proliferation measured with CellTiter Glo shows no significant differences between cells reconstituted with the *BAP1* synonymous mutation and the other vectors for UMRC-6 and TFK-1 cells. Data is the average ± SD of three independent experiments.

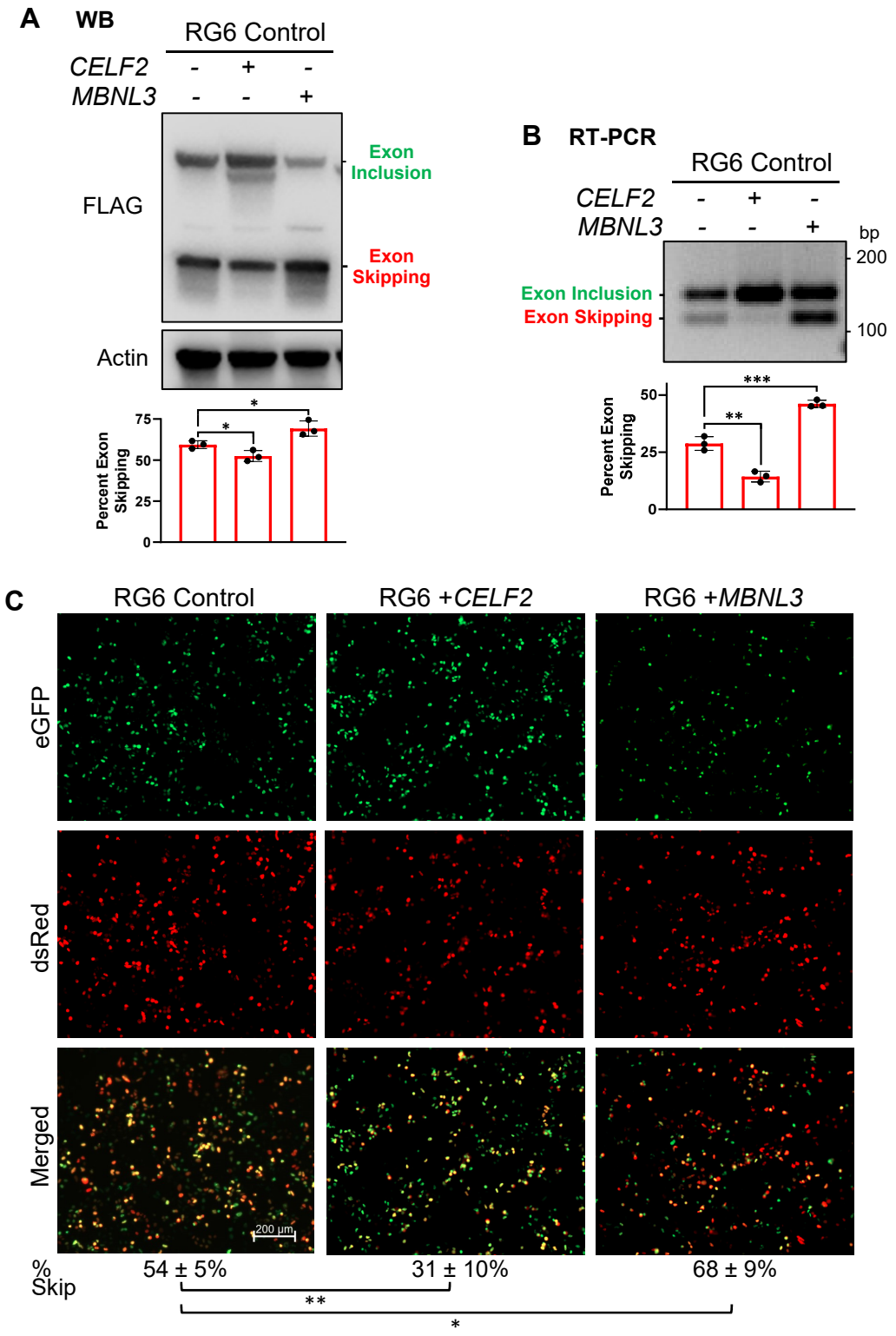

Figure S4. RG6 minigene provides a reliable readout for *in vivo* splicing, Related to Figure 3. **A-C**, HeLa cells transiently transfected with the minigene reporter (RG6) control showed similar levels of exon inclusion and skipping, as indicated by western blotting (WB) of Flag-tagged proteins (**A**), RT-PCR (**B**) and fluorescence microscopy (**C**). Co-expression of Flag-*CELF2* enhanced exon inclusion whereas co-expression of Flag-*MBNL3* enhanced exon skipping, as previously reported by Orengo and colleagues (2006). Quantification of western blotting and RT-PCR represents the average ± SD of three independent experiments. *, *P*<0.05; **, *P*<0.01; ***, *P*<0.001.

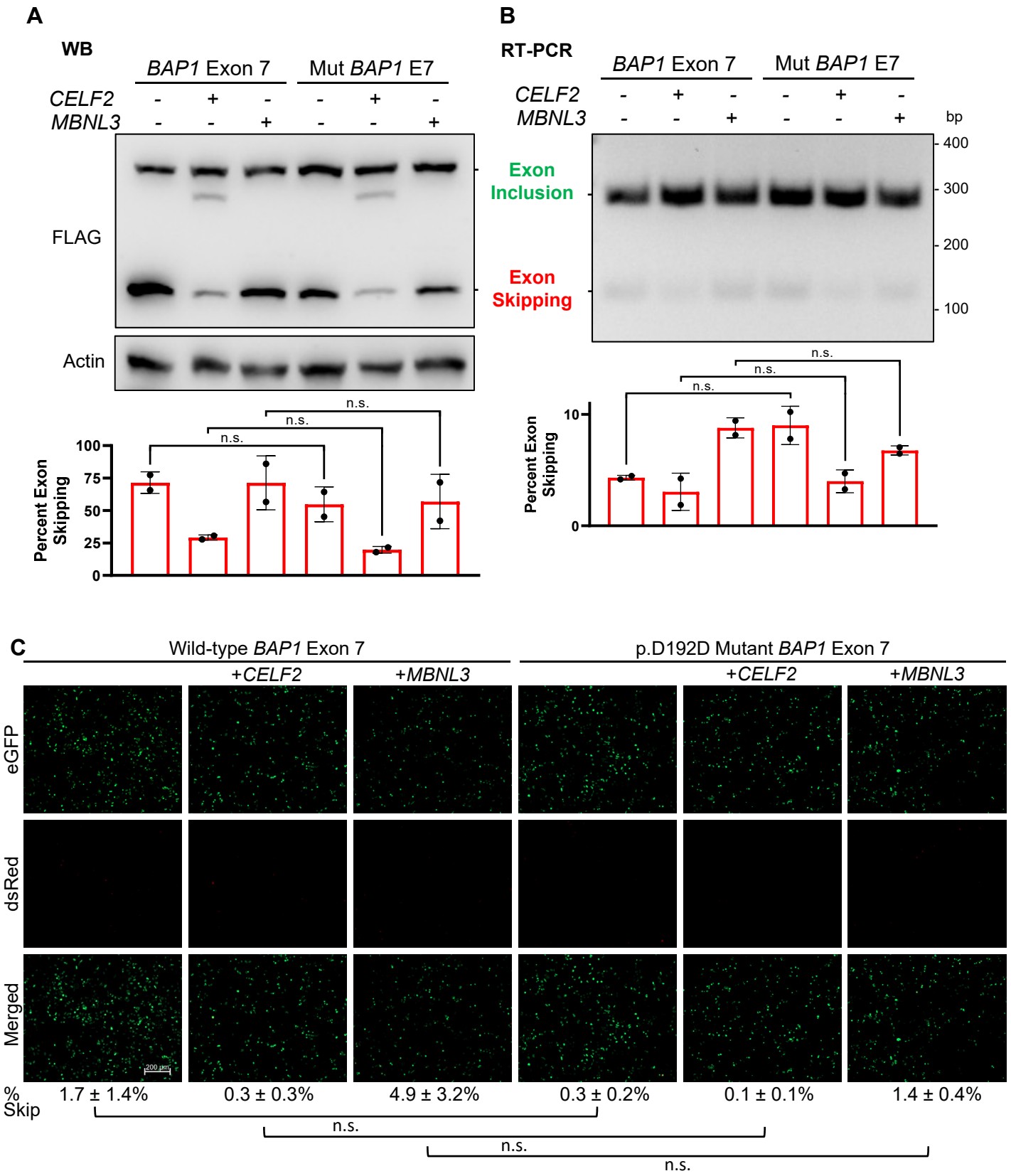

Figure S5. The c.576C>T, p.D192D synonymous *BAP1* mutation in exon 7 near the donor splice site do not affect splicing, Related to Figure 3. **A-C**, BAP1 exon 7 is largely included regardless of the c.576C>T, p.D192D synonymous mutation in HeLa cells transiently transfected with a minigene reporter, as indicated by Western blotting (WB) of Flag-tagged proteins (**A**), RT-PCR (**B**) and fluorescence microscopy (**C**). Quantifications are the average ± SD of two independent experiments. n.s., not significant.

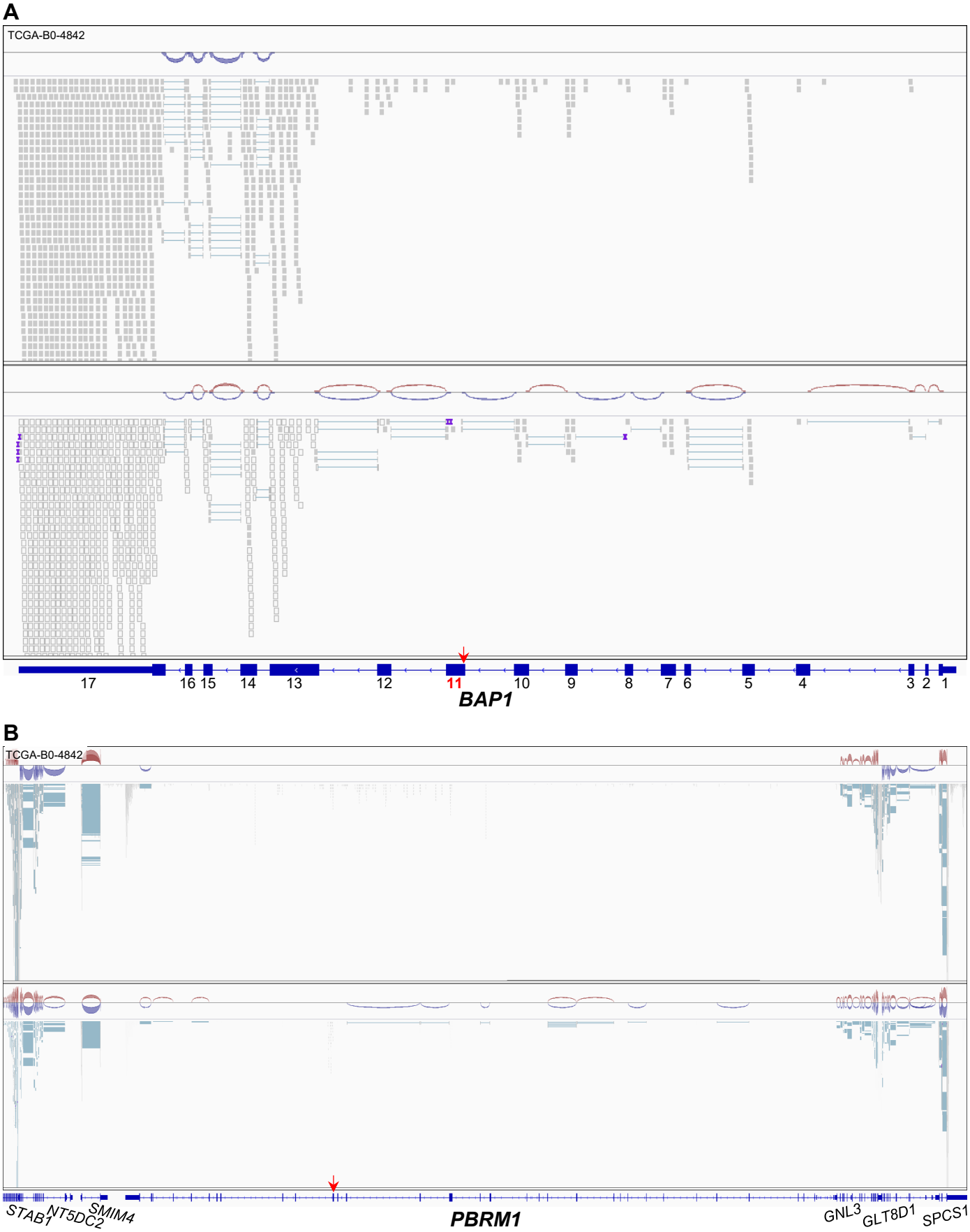

Figure S6. Index patient shows low RNA-Seq reads for *BAP1* and *PBRM1* but not adjacent genes, consistent with nonsense-mediated mRNA decay, Related to Figure 4. RNA-Seq data from two tumor samples was obtained from KIRC-TCGA and visualized with IGV. Red arrow indicates somatic mutation.

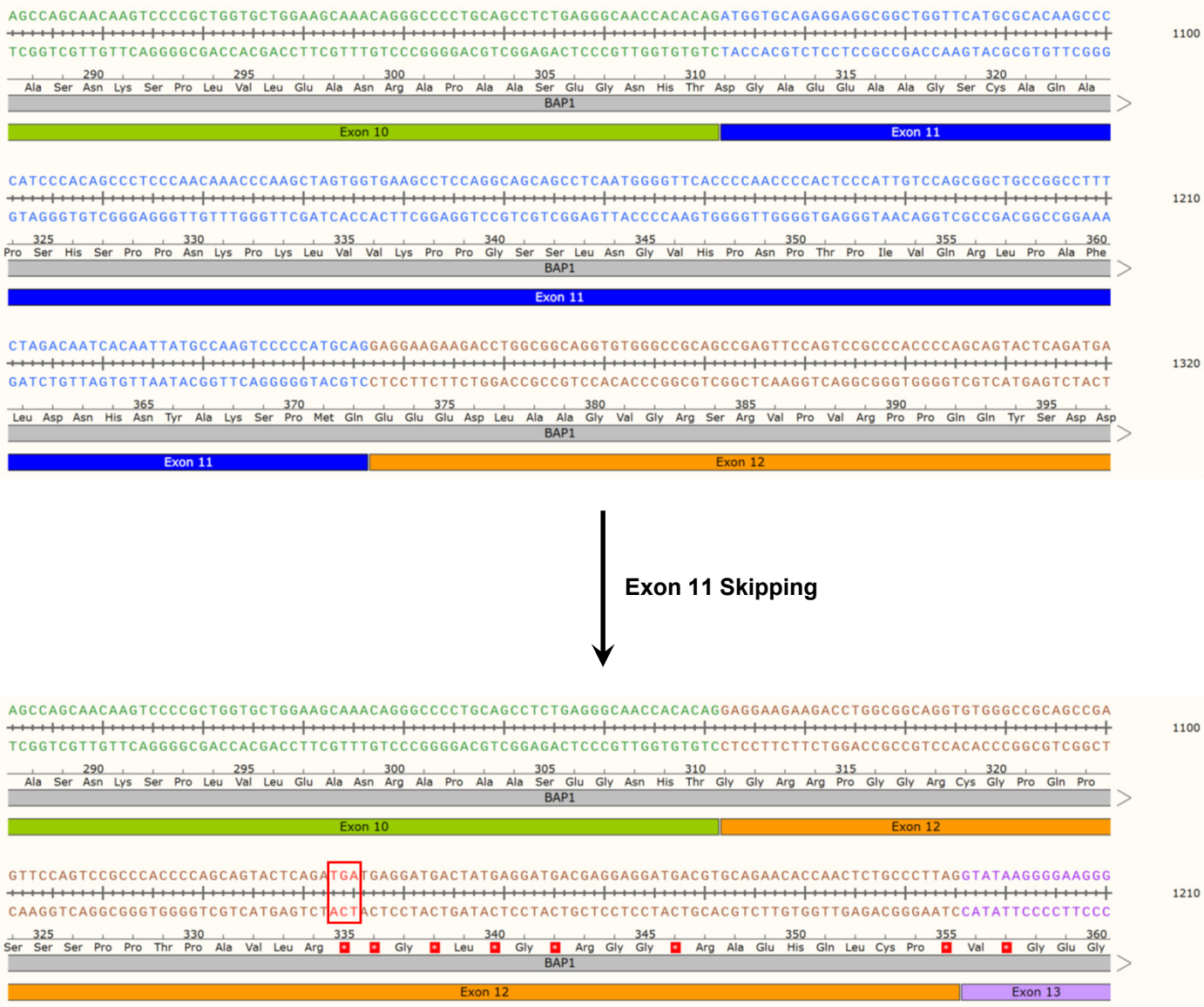

Figure S7. *BAP1* exon 11 skipping results in frameshift and premature stop codon at amino acid 335, Related to Figure 4. *BAP1* sequence was analyzed using SnapGene.

Table S1. List of primers, Related to Figures 2 and 3.

Primer name	Sequence 5'-3'
Primers for cloning BAP1	
BamHI-Kozak-BAP1_F	CGCGGATCCGCCACCATGAATAAGGGCTGGCTGGAG
EcoRI-Stop-HA-BAP1_RC	CCGGAATTCTCAAGCGTAATCTGGAACATCGTATGGGTACT GGCGCTTGGCCTTGTAGGG
Primers for the generation of the p.G312G mutation by site-directed mutagenesis	
BAP1_(G312G)-SDM_F	GGCAACCACACAGATGGGGCAGAGGAGGCGGCT
BAP1_(G312G)-SDM_RC	AGCCGCCTCCTCTGCCCCATCTGTGTGGTTGCC
Primers for cloning BAP1 Exon 7	
BamHI-BAP1_E7_F	CGCGGATCCCCCGAGCCACGCCACCTCC
EcoRI-BAP1_E7_RC	CCGGAATTCATGGTCAATGGGGTAGACC
EcoRI-BAP1-Mutant_E7_RC	CCGGAATTCATGATCAATGGGGTAGACC
Primers for cloning BAP1 Exon 11	
BamHI-BAP1_E11_F	CGCGGATCCGATGGTGCAGAGGAGGCGGCTG
BamHI-BAP1-Mutant_E11_F	CGCGGATCCGATGGGGCAGAGGAGGCGGCTG
EcoRI-BAP1_E11_RC	CCGGAATTCCTGCATGGGGGACTTGGCAT
Primers for RT-PCR	
RG6_RT-PCR_Fwd	CAAAGTGGAGGACCCAGTACC
RG6_RT-PCR_Rev	GCGCATGAACTCCTTGATGAC

TRANSPARENT METHODS

KEY RESOURCES TABLE

REAGENT or RESOURCE	SOURCE	IDENTIFIER
Antibodies		
Rabbit polyclonal anti-human 4E-BP1	Cell Signaling Technology	Cat# 9452; RRID: AB_331692
Mouse monoclonal anti-human ß-Actin HRP	Santa Cruz	Cat# sc-47778 HRP; RRID: AB_2714189
Mouse monoclonal anti-human BAP1 (C-4)	Santa Cruz	Cat# sc-28383; RRID: AB_626723
Rabbit polyclonal anti-human Histone H2A	Sigma-Aldrich	Cat# ABE327
Rabbit polyclonal anti-human p70 S6 Kinase	Cell Signaling Technology	Cat# 9202; RRID: AB_331676
Rabbit polyclonal anti-human Phospho-p70 S6 Kinase (Thr389)	Cell Signaling Technology	Cat# 9205; RRID: AB_330944
Rabbit polyclonal anti-human Phospho-S6 Ribosomal Protein (Ser240/244)	Cell Signaling Technology	Cat# 2215; RRID: AB_331682
Rabbit monoclonal anti-human S6 Ribosomal Protein (5G10)	Cell Signaling Technology	Cat# 2217; RRID: AB_331355
Mouse monoclonal anti-human Ubiquityl-Histone H2A (H2A-Ub) (E6C5)	Millipore	Cat# 05-678; RRID: AB_309899
Mouse monoclonal anti-Flag (M2)	Sigma-Aldrich	Cat# F3165; RRID: AB_259529
Goat polyclonal anti-mouse IgG (H + L) HRPO	Jackson ImmunoResearch	Cat# 115-035-003; RRID: AB_10015289
Goat polyclonal anti-rabbit IgG (H + L) HRPO	Jackson ImmunoResearch	Cat# 111-035-003; RRID: AB_2313567
Chemicals, Peptides, and Recombinant Proteins		
DMEM, High Glucose	Gibco	Cat# 41965062
Fetal Bovine Serum (FBS)	Gibco	Cat# 10500064
Hanks' Balanced Salt Solution (HBSS)	Gibco	Cat# 24020117
HotStarTaq Plus MasterMix	Qiagen	Cat# 203643
Hygromycin B	Santa Cruz	Cat# sc-29067
Platinum *Taq* DNA Polymerase High Fidelity	Life Technologies	Cat# 11304011
RPMI 1640 Medium, GlutaMAX Suppl.	Gibco	Cat# 61870044
T4 DNA Ligase	New England Biolabs	Cat# M0202
Critical Commercial Assays		
AllPrep DNA/RNA Mini Kit	Qiagen	Cat# 80204
CellTiter Glo Luminescent Viability Assay	Promega	Cat# G7573
High-Capacity cDNA Reverse Transcription kit	Applied Biosystems	Cat# 4368814
QuickChange II XL Site-Directed Mutagenesis Kit	Agilent Technologies	Cat# 200521
*Trans*IT-LT1 Transfection Reagent	Mirus	Cat# 731-0029
Deposited Data		
Level 3 RNA-Seq, segmented DNA copy numbers (GRCh37/hg19) and RPPA data. Legacy BAM files for DNA and RNA sequencing data	TCGA Data Portal	https://portal.gdc.cancer.gov

REAGENT or RESOURCE	SOURCE	IDENTIFIER
Experimental Models: Cell Lines		
HEK-293GP (Phoenix-GP)	Laboratory of Stefan Fröhling	RRID: CVCL_H718
HeLa	ATCC	Cat# CCL-2; RRID: CVCL_0030
TFK-1	Laboratory of Stephanie Rössler	RRID: CVCL_2214
UMRC-6	Sigma-Aldrich	Cat# 08090513; RRID: CVCL_2741
Oligonucleotides		
Primers for *BAP1* cloning	This paper	Table S1
Primers for site-directed mutagenesis	This paper	Table S1
Primers for *BAP1* exon 7 cloning	This paper	Table S1
Primers for *BAP1* exon 11 cloning	This paper	Table S1
Primers for RT-PCR	Orengo et al. (2006)	Table S1
Recombinant DNA		
pBABE-hygro	Morgenstern and Land (1990)	https://www.addgene.org/1765
pBABE-hygro-BAP1-HA	This paper	https://www.addgene.org/154020
pBABE-hygro-BAP1-C91S-HA	This paper	https://www.addgene.org/154021
pBABE-hygro-BAP1-G312G-HA	This paper	https://www.addgene.org/154022
pCMV-VSV-G	Stewart et al. (2003)	https://www.addgene.org/8454
FlagETR3 (CELF2)	Orengo et al. (2006)	https://www.addgene.org/96900
FlagMBNL3	Orengo et al. (2006)	https://www.addgene.org/96901
RG6	Orengo et al. (2006)	https://www.addgene.org/80167
RG6-BAP1_E7	This paper	https://www.addgene.org/154023
RG6-BAP1_E7-D192D	This paper	https://www.addgene.org/154024
RG6-BAP1_E11	This paper	https://www.addgene.org/154025
RG6-BAP1_E11-G312G	This paper	https://www.addgene.org/154026
Software and Algorithms		
GraphPad Prism 8	GraphPad Software	https://www.graphpad.com/scientific-software/prism
IBM SPSS Statistics 25.0	IBM	https://www.ibm.com/products/spss-statistics
ImageJ	NIH	https://imagej.nih.gov/ij/
Integrative Genomics Viewer (IGV)	Broad Institute	https://software.broadinstitute.org/software/igv
IGV Crawler 2.0	DKFZ Omics IT & Data Management Core Facility	https://github.com/DKFZ-ODCF/igv-crawler
Mutation Surveyor 5	Softgenetics	https://softgenetics.com/mutationSurveyor.php
SnapGene 5	GSL Biotech	https://www.snapgene.com
Zeiss ZEN 3.0	Zeiss	https://www.zeiss.com/microscopy/int/products/microscope-software/zen-lite.html

EXPERIMENTAL MODEL AND SUBJECT DETAILS

Subject details

The index patient involves a 73-year-old Caucasian woman from KIRC-TCGA (TCGA-B0-4842), who died 56 months after diagnosis and was homozygous for a nonsense mutation in *PBRM1* and a somatic synonymous mutation in *BAP1* near the acceptor slice site of exon 11. KIRC-TCGA patients with mutations

in the acceptor splice site of *BAP1* exon 11 comprise patient TCGA-BP-4798, a 74-year-old Caucasian man with an additional *TP53* missense mutation and distant metastasis at presentation, who died almost 11 months after diagnosis, and patient TCGA-CZ-5985, a 58-year-old Caucasian man, who was still alive 65 months after diagnosis. Further information on the other KIRC-TCGA patients can be found elsewhere (Creighton et al., 2013; Ricketts et al., 2018).

Ethical issues

NCI and NHGRI developed a set of policies to protect the privacy of participants donating specimens to TCGA (https://www.cancer.gov/about-nci/organization/ccg/research/structural-genomics/tcga/history/policies).

METHOD DETAILS

Bioinformatics Analyses

RNA-Sequencing (RNA-Seq), segmented DNA copy numbers (GRCh37/hg19) and reverse phase protein array (RPPA) data from clear-cell renal cell carcinoma (KIRC) patients from The Cancer Genome Atlas (TCGA) were downloaded from the Genomic Data Commons (GDC) data portal (https://portal.gdc.cancer.gov). Updated mutation and survival data was obtained from Ricketts et al. (2018) and analyzed as previously described (Peña-Llopis et al., 2016). Gene expression levels were estimated by the RNA-Seq Expectation-Maximization (RSEM) normalization method and log2 transformed. Whole-exome sequencing (WES) and RNA-Seq raw BAM files from legacy (GRCh37/hg19) KIRC-TCGA were downloaded from the GDC data portal and indexed using IGV Crawler v2.0, an open source tool by the DKFZ Omics IT & Data Management Core Facility (ODCF, https://github.com/DKFZ-ODCF/igv-crawler). Genomic data was visualized with the Integrative Genomics Viewer (IGV, https://software.broadinstitute.org/software/igv).

Plasmids

Full-length human wild-type *BAP1* and the p.C91S mutant was cloned by PCR amplification with Platinum Taq DNA polymerase (Life Technologies, 11304011) of previous vectors (Machida et al., 2009) using primers with BamHI and EcoRI restriction sites (Table S1) and ligated into pBABE-hygro (Morgenstern and Land, 1990) (Addgene #1765) to generate C-terminal HA-tagged *BAP1* (pBABE-hygro-*BAP1*-HA) and its corresponding p.C91S mutant (pBABE-hygro-*BAP1*-C91S-HA). The c.936T>G, p.G312G *BAP1* mutation was introduced into pBABE-hygro-*BAP1*-HA using the QuickChange II XL Site-Directed Mutagenesis Kit (Agilent Technologies, 200521) and specific primers (Table S1) to obtain pBABE-hygro-*BAP1*-G312G-HA.

Wild-type and mutant exon 7 and exon 11 of *BAP1* were designed with SnapGene (GSL Biotech) and cloned by PCR amplification with Platinum Taq DNA polymerase (Life Technologies, 11304011) using primers with BamHI and EcoRI restriction sites (Table S1) and ligated into RG6 plasmid (Orengo et al., 2006) (Addgene #80176) with T4 DNA Ligase (New England Biolabs, M0202). All plasmids generated in this study were confirmed by Sanger sequencing (Eurofins Genomics) with Mutation Surveyor (Softgenetics) and have been deposited to Addgene (Addgene IDs 154020-154026).

Cell Culture

The clear-cell renal cell carcinoma cell line with a *BAP1* frameshift deletion (Peña-Llopis et al., 2012), UMRC-6, was obtained from Sigma-Aldrich. The cholangiocarcinoma cell line with a *BAP1* nonsense mutation, TFK-1, was a generous gift from Dr. Stephanie Rössler (University Hospital Heidelberg). HEK-293GP (Phoenix-GP) was kindly provided by Prof. Stefan Fröhling (DKFZ, Heidelberg). HeLa cells were obtained from ATCC. Cells were maintained in Dulbecco's Modified Eagle's Medium (DMEM) (Gibco, 41965062) supplemented with 10% Fetal Bovine Serum (FBS) (Gibco, 10500064) and 1% (v/v) Penicillin/Streptomycin in a humidified incubator at 37 °C and 5% CO_2, with the exception of the TFK-1 cells, which were grown in RPMI (Gibco, 61870044) supplemented with 10% FBS and 1% Pen/Strep. Cells were routinely tested for mycoplasma by PCR. Cell lines were authenticated using Multiplex Cell Authentication by Multiplexion (Heidelberg, Germany) as described (Castro et al., 2013).

Retroviral Transduction

To stably express *BAP1* in BAP1-null cell lines, we generated retroviruses by transfecting the HEK-293GP cells with pVSV-G envelope plasmid (Stewart et al., 2003) (Addgene #8454) and the pBabe-hygro constructs using *Trans*IT-LT1 Transfection Reagent (Mirus, 731-0029) according to the manufacturer's instructions. Media were collected and filtered through a 0.45-µm syringe filter (Corning, 431220). UMRC-6 and TFK-1 cells were transduced with retroviruses and 48 h later selected with 250 µg/ml hygromycin B (Santa Cruz, sc-29067) for at least a week.

BAP1 Protein Stability Assay

UMRC-6 and TFK-1 cells were treated with 80 and 10 µg/ml of cycloheximide, respectively, for 6, 12 and 24 h. Cells were washed with ice-cold PBS and harvested for western blotting.

In Vivo Splicing Assay

We transfected HeLa cells when reaching 80% confluency in a 6-well plate with 2.5 µg of the cloned RG6 constructs using Opti-MEM reduced-serum medium (Life Technologies) and *Trans*IT-LT1 Transfection Reagent (Mirus, 731-0029) according to the manufacturer's instructions. Flag-tagged *CELF2* (Addgene #96900) and Flag-*MBNL3* (Addgene #96901) were also co-expressed to promote exon inclusion and exclusion, respectively (Orengo et al., 2006). Cells were observed under a fluorescence inverted microscope (Zeiss Primovert, Oberkochen, Germany) using an excitation of 488 nm to detect eGFP and 594 nm to detect dsRed and quantified with Zeiss ZEN 3.0 microscope software. Cells were harvested 48 h after transfection to obtain proteins for western blotting and RNA for RT-PCR.

Western blotting

Cells were harvested in Protein Lysis buffer (Peña-Llopis and Brugarolas, 2013) containing Halt protease inhibitors (Fisher Scientific, 11834101) and Halt phosphatase inhibitors (Fisher Scientific, 11814101) for 10 minutes at 4 °C. Upon clearing of the lysate, proteins were quantified with Bradford protein assay (Bio-Rad, 500-0006) and boiled at 95 °C for 10 min in 4x Laemmli Sample Buffer (Bio-Rad, 1610747). Samples were loaded in 4-15% Mini-PROTEAN TGX Precast Protein Gels (Bio-Rad, 4561084DC) and run in 1x SDS running buffer in a Mini-PROTEAN Tetra Cell (Bio-Rad) at 120 V for approximately 1 h. Samples were then transferred to a 0.2-µm nitrocellulose membrane using a semidry Trans-Blot Turbo Transfer System (Bio-Rad). Membranes were blocked in 5% BSA in TBS-T on a rocking platform for 1 h at room temperature and incubated overnight with primary antibodies diluted in 5% BSA/TBS-T containing 0.05% sodium azide on a digital tube roller (Roth) at 4 °C. Primary and secondary antibodies are listed in the Key Resources Table. Membranes were developed with ECL Prime Western Blotting Detection Reagent (GE Healthcare, RPN2236) and visualized in a ChemiDoc MP Image System (Bio-Rad). Exon inclusion and exclusion were quantified with ImageJ and means compared using a two-tailed Student's *t* test (or a Welch's *t* test if unequal variances).

Reverse-Transcribed PCR (RT-PCR)

Cells were washed with PBS 48 h after transfection and harvested with RLT Buffer (Qiagen). RNA was extracted using RNeasy columns (Qiagen, 80204) and cDNA from 1 µg RNA was synthesized using the High-Capacity cDNA Reverse Transcription kit (Applied Biosystems, 4368814) according to the manufacturer's instructions. PCR was performed with 2 µl of cDNA and HotStarTaq Plus MasterMix kit (Qiagen, 203643) for 20 cycles (30 sec at 94 °C, 30 sec at 60 °C and 1 min at 72 °C) using a T100 Thermal Cycler (Bio-Rad). PCR products were analyzed by 2% agarose gel electrophoresis in 1x TAE buffer. Exon inclusion and exclusion were quantified with ImageJ and means compared using a two-tailed Student's *t* test (or a Welch's *t* test if unequal variances).

Histone Purification

Histones were isolated by acid extraction as previously described (Peña-Llopis et al., 2012). Briefly, cells were washed with PBS, scraped and centrifuged at 1,000·*g* for 5 min. Cell pellets were resuspended in 400 µl of cold 0.4 M HCl and rocked at 4 °C for at least 30 min. Extracts were pelleted after spinning 10 min at 16,000·*g*, and supernatants were precipitated with 10% trichloroacetic acid and analyzed by western blotting.

Starvation studies

Cells were seeded in 6-well plates the day before the experiment. Media was changed in untreated samples by full media containing 10% FBS. For starved samples, cells were washed twice with PBS and incubated with Hanks' Balanced Salt Solution (HBSS) (Gibco, 24020117) for 1 or 3 h.

Cell Proliferation Assay

500 cells/well of each cell line were seeded in 384-well plates in triplicate in their usual culture medium using a total volume of 30 µl per well. Every 24 h, cell viability was assessed using the CellTiter Glo Luminescent Viability Assay (Promega, G7573) according to the manufacturer's protocol. Briefly, CellTiter Glo (CTG) reagent was diluted 1:4 in DPBS before use. Assay plates were removed from the incubator at 37 °C and incubated for 30 min at room temperature. 30 µl/well of diluted CTG reagent were added to the assay plate and the plate was shaken for 2 min for full cell lysis. The assay plate was incubated for 8 min at room temperature in the dark and luminescence was measured for 500 ms/well using the Spark 10M plate reader (Tecan) and the software Spark Control (Tecan, Version 1.2). Viability data was normalized to day 0 and graphs were plotted using GraphPad Prism 8.

Statistical Analyses

Overall survival from KIRC-TCGA was determined from the date of diagnosis to time to death or last follow-up, using updated mutation and survival data from Ricketts et al. (2018). Kaplan-Meier survival curves were compared by log-rank tests using IBM SPSS Statistics 25.0. To compare *BAP1* gene expression and protein expression of the index patient to the *BAP1* and/or *PBRM1* subgroups of KIRC-TCGA, one-sample *t* tests were conducted in IBM SPSS Statistics 25.0. Microsoft Excel and GraphPad Prism 8 were used to calculate the rest of statistical analyses. Data is representative of three independent experiments, except two experiments for the splicing of *BAP1* exon 7. Exon skipping quantification was displayed as mean ± SD and *P* values were calculated using a two-tailed Student's *t* test when equal variances or a Welch's *t* test when unequal variances. A cumulative binomial distribution was used to calculate the probability of having two splice-site mutations in the acceptor splice site of *BAP1* exon 11 out of 8 splice-site mutants from KIRC-TCGA.

SUPPLEMENTAL REFERENCES

Castro, F., Dirks, W.G., Fahnrich, S., Hotz-Wagenblatt, A., Pawlita, M., and Schmitt, M. (2013). High-throughput SNP-based authentication of human cell lines. Int. J. Cancer *132*, 308-314.

Creighton, C.J., Morgan, M., Gunaratne, P.H., Wheeler, D.A., Gibbs, R.A., Gordon Robertson, A., Chu, A., Beroukhim, R., Cibulskis, K., Signoretti, S.*, et al.* (2013). Comprehensive molecular characterization of clear cell renal cell carcinoma. Nature *499*, 43-49.

Machida, Y.J., Machida, Y., Vashisht, A.A., Wohlschlegel, J.A., and Dutta, A. (2009). The deubiquitinating enzyme BAP1 regulates cell growth via interaction with HCF-1. J. Biol. Chem. *284*, 34179-34188.

Morgenstern, J.P., and Land, H. (1990). Advanced mammalian gene transfer: high titre retroviral vectors with multiple drug selection markers and a complementary helper-free packaging cell line. Nucleic Acids Res. *18*, 3587-3596.

Orengo, J.P., Bundman, D., and Cooper, T.A. (2006). A bichromatic fluorescent reporter for cell-based screens of alternative splicing. Nucleic Acids Res. *34*, e148.

Peña-Llopis, S., and Brugarolas, J. (2013). Simultaneous isolation of high-quality DNA, RNA, miRNA and proteins from tissues for genomic applications. Nat. Protoc. *8*, 2240-2255.

Peña-Llopis, S., Vega-Rubín-de-Celis, S., Liao, A., Leng, N., Pavía-Jiménez, A., Wang, S., Yamasaki, T., Zhrebker, L., Sivanand, S., Spence, P.*, et al.* (2012). BAP1 loss defines a new class of renal cell carcinoma. Nat. Genet. *44*, 751-759.

Peña-Llopis, S., Wan, Y., and Martinez, E.D. (2016). Unique epigenetic gene profiles define human breast cancers with poor prognosis. Oncotarget *7*, 85819-85831.

Ricketts, C.J., De Cubas, A.A., Fan, H., Smith, C.C., Lang, M., Reznik, E., Bowlby, R., Gibb, E.A., Akbani, R., Beroukhim, R.*, et al.* (2018). The Cancer Genome Atlas Comprehensive Molecular Characterization of Renal Cell Carcinoma. Cell Rep. *23*, 313-326.

Stewart, S.A., Dykxhoorn, D.M., Palliser, D., Mizuno, H., Yu, E.Y., An, D.S., Sabatini, D.M., Chen, I.S., Hahn, W.C., Sharp, P.A.*, et al.* (2003). Lentivirus-delivered stable gene silencing by RNAi in primary cells. RNA *9*, 493-501.